Electron temperature and heating processes in a dynamic plasma of a high-power diode

Y. Maron, M. Sarfaty, L. Perelmutter, O. Zahavi, M. E. Foord, and E. Sarid
Physics Department, Weizmann Institute of Science, Rehovot, 76 100, Israel
(Received 27 January 1988; revised manuscript received 10 April 1989)

Using time-dependent measurements and calculations of line-intensity ratios, we have determined the electron temperature of a surface flashover anode plasma in an intense ion diode to be 5–8 eV. The electron temperature was determined independently from C III, Mg II, and Al III line intensities. The calculations accounted for the continuous particle flow from the anode surface into the plasma using the measured electron density. Furthermore, the electron-temperature gradient in the plasma was observed and found to be <1 eV/mm. The assumption that the plasma conductivity is classical, resulting in the electron heating being dominated by the currents induced in the plasma by the electron flow in the diode gap, was found to be in clear disagreement with the observed temperature gradient. The use of an anomalous plasma conductivity that is $\simeq 10\times$ lower than the classical conductivity, which was previously suggested based on the magnetic field penetration into the plasma and the plasma expansion against the magnetic field, yields electron heating dominated by the pressure-driven current in the plasma. This can explain the electron heating and the electron-temperature gradient observed.

I. INTRODUCTION

Determination of the electron temperature in plasmas formed in pulsed ($\simeq 100$ ns) high-voltage high-power devices is of major importance since this temperature significantly influences several characteristics in the plasma behavior that usually play an important role in the device operation. Examples of these devices are ion-beam diodes,[1–3] relativistic electron-beam diodes,[4] plasma erosion switches for high-current switching,[5,6] magnetically insulated lines for power transmission,[7] and magnetrons for high-power microwave generation.[8] In these devices the plasma electron temperature affects the electron collisionality, which influences the plasma expansion across the magnetic field. It also determines the ionization rates in the plasma which strongly affect the time-dependent concentrations of neutral particles and various charge states in the plasma, and through them the composition of the extracted ion beams. Finally, the plasma conductivity, which depends on the electron temperature, determines the time-dependence penetration of magnetic fields into the plasma and the plasma Ohmic heating.

Determination of the electron temperature in plasmas in such short-pulse devices is difficult. Such plasmas, with electron temperatures of a few electron volts and electron densities of $10^{14}-10^{17}$ cm^{-3}, undergo rapid ionization during the pulse, remaining far from ionization equilibrium, with the excited levels being populated mostly through excitations from the ground state, as discussed by Griem.[9] In these cases, the relative populations of excited levels used for the determination of the electron temperature are significantly different from steady-state values. A demonstration of this phenomenon is that for high levels in the atom partial local thermal equilibrium[9] (LTE) does not exist even though the inelastic electron collisions with the excited atom are much more frequent than radiation processes.[9,10]

An additional complication in this problem results from continuous flow of material into the plasma throughout the pulse from the plasma source or from the surface over which the plasma evolves. The material ejection into the plasma continuously modifies the ground-state and the excited-level population densities, which can result in a continuous modification of the excited-level population ratios, used for the determination of the electron temperature. It will be shown in Sec. IV B that the excited-level population ratio for the present plasma parameters can be different by a factor of 10 or more from steady-state calculations. Therefore, using collisional-radiative steady-state calculations of the atomic-level populations for determining the electron temperature from measured line-intensity ratios can give misleading results. Finally, for calculating the time-dependent populations of excited levels in such transient plasmas, knowledge of the electron density is essential.

Prior to the measurements reported here, attempts to obtain the electron temperature in pulsed-power plasmas have been made by Johnson and co-workers[11,12] and Hinshelwood.[13] In Ref. 11 the temperature of the anode plasma in a 900-kV, 400-kA, 100-ns pulsed magnetically insulated ion diode was estimated from measurements of the charge-state ratios in the extracted ion beam, based on a coronal model for the ionization distribution in the plasma. In Ref. 12 intensity ratios of C III and C IV lines were used to estimate the temperature in the anode plasma in a 700-kV, 400-kA, 100-ns magnetically insulated diode assuming a LTE model. Hinshelwood[13] used C III and Al III line intensities and steady-state calculations to study the electron temperature in the cathode plasma in a 250-kV, 50-kA, 80-ns electron-beam diode. To our knowledge, no allowance for the level-population time dependence and for the continuous material flow into the plasma has been made.

For the anode plasma in high-power diodes it was usu-

ally assumed that the electron temperature T_e is a few electron volts. However, in this temperature range the ionization rates are very sensitive to the value of T_e, and thus an experimental determination of T_e is essential for estimating the charge-state distribution in the plasma.

Here we report the determination of the electron temperature in the surface-flashover anode plasma in a planar magnetically insulated ion diode powered by a $\simeq 100$-ns pulse by observing line intensities of various species as a function of time. The line intensities are compared with intensities calculated by a *time-dependent* collisional-radiative code which predicts the time evolution of the atomic-level populations. The temporal variations in the line-intensity ratios are calculated taking into account the continuous material supply from the anode surface to the plasma. This material flow has been quantitatively investigated for the surface-flashover anode plasma studied here and is reported in a companion paper.[14] The electron temperature was determined for times in which the line-intensity ratios were calculated and observed to vary slowly, and were relatively insensitive to details of the continuous material supply. On the basis of these calculations we determined the electron temperature in the second half of the pulse.

Using two spectroscopic systems we observed the intensities of two lines in a single discharge. These simultaneous measurements enabled us to obtain line-intensity ratios free of ambiguity due to shot-to-shot irreproducibilities that often characterize pulsed-power experiments. Also, using one line intensity as a reference we could normalize several line intensities obtained from repeated discharges for the same charge state, thus reliably obtaining the population of several levels, required for consistency checks of the electron-temperature determination. Furthermore, high spectral resolution ($\simeq 0.1$ Å) was required in order to reliably discriminate against impurity lines. The electron density, necessary for the calculations, was obtained as a function of time from our observations[15] of the Stark and Doppler broadening of H_β and H_α lines.

The electron temperature was determined independently from line intensities of three species: Mg II, Al III, and C III. The results for all species yielded T_e between 5 and 8 eV.

The Ohmic electron heating in the plasma is then analyzed. The currents in the plasma result from induction of the electron flow in the diode acceleration gap and from the plasma pressure gradient in the magnetic field. The latter was shown in Ref. 15 to be important due to the relatively high ion temperature, a few tens of electron volts, as observed from line Doppler broadening. If a classical conductivity[16] were assumed, the electron heating would be dominated by the relatively large current induced by the electron flow in the diode gap. Using the measured electron density,[15] calculations show that this diamagnetic heating should result in an electron-temperature gradient in the plasma of about 5 eV/mm. This temperature gradient cannot be reduced by thermal convection or conduction because of the strong electron magnetization (the magnetic field was observed[17] to penetrate the plasma early in the pulse). This predicted large temperature gradient was found to be in clear contradiction to spatially resolved line-intensity–ratio measurements that showed rather uniform temperature over the plasma (with spatial variations $\lesssim 1$ eV/mm, see Sec. IV D).

In order to explain the temperature uniformity, we use our suggestion[15,17] that the plasma conductivity is anomalously $\simeq 10\times$ lower than the classical conductivity. With this anomalous conductivity the currents induced in the plasma by the electron flow in the gap are shown to be much smaller and more uniform. The electron heating is then dominated by the currents due to the plasma pressure gradient. This heating is likely to result in small temperature gradients in the plasma, especially since in the case of anomalous conductivity the characteristic time of the electron thermal convection against the magnetic field decreases to about the pulse length.

The electron Ohmic heating due to the total pressure-driven current in the plasma assuming this anomalous plasma conductivity is estimated. Together with the electron heating due to elastic collisions with the hotter ions,[15] this heating, averaged over the plasma, is shown to about balance the average electron cooling due to inelastic collisions with the plasma particles[14] and thermal convection to the anode surface. This is consistent with the approximately constant electron temperature observed.

II. EXPERIMENTAL ARRANGEMENT

The plasma in these experiments was produced by a flashover of the dielectric anode surface in a planar magnetically insulated gap as described in Ref. 15. The magnetic field B_z, which inhibits the electron flow across the 8-mm-wide diode gap, was varied in these experiments between 5.5 and 9 kG. The active dielectric anode was made of impurity doped epoxy that filled grooves along the z direction in an aluminum plate. The height in the y direction of the active anode was 6 cm and its length in the z direction was 8 cm.

The diode was powered by a 270-kV, 90-ns pulse delivered by an LC generator coupled to a 1-Ω water line. The use of a low-impedance line allowed the electron temperature to be examined for various applied magnetic fields with the voltage pulse height on the relatively high-impedance (usually $\simeq 20$ Ω) diode being essentially independent of the applied magnetic field. A description of the diode and the voltage and current waveforms are given in Ref. 15.

Light was collected from the anode plasma along the z direction, parallel to the magnetic field lines (as shown in Fig. 1). Fused-silica optics were used to split the light and direct each portion to a spectrometer input slit through the demagnifying lens (L_1 or L_2). Beam splitters with transmission coefficients from 30% to 93% were used in order to minimize the attenuation of weak lines. These measurements integrated over the active anode length. The spatial resolution in the x direction (the anode-cathode–gap direction) was determined by the spectrometer input-slit width, the demagnification factor of the lens (L_1 or L_2), and the anode length (due to de-

focusing along the line of sight). The spatial resolution was varied in the experiments between 0.5 and 3 mm. By allowing our optical system to collect light only from a 3.5-cm-high portion of the anode plasma centered at the anode vertical center, these measurements were not affected by light from the cathode-vane plasma or from the plasma on the aluminum anode stalk.

For the line-intensity measurements in the present experiments it was essential to observe the line spectral profile with a high spectral resolution in order to reliably separate the observed lines from nearby impurity lines. For a few lines a resolution of 0.1 Å was required. This was obtained by using a magnifying cylindrical lens (CL) at the spectrograph output followed by a rectangular fiber-bundle array coupled to photomultiplier tubes as described in Ref. 15. The line intensity was then obtained as a function of time, with a temporal resolution of 5 ns, by integrating over the line spectral profile observed by six fiber channels. Absolute intensity calibration of the system over the entire spectrum was performed for each fiber channel using two intensity-calibrated lamps for the visible and the uv region that overlapped in the 3000–4000-Å region. Although an absolute calibration was not necessary for this study, it provided the relative sensitivity of the two spectroscopic systems as a function of wavelength. The diode window was periodically cleaned from discharge blow off in order to maintain its transmission characteristics over the entire spectrum.

The epoxy used for the dielectric anode was mixed with powders of MgF_2, CaF_2, and $AlNaSiO_3$, each constituting 20% by weight of the entire mixture. This allowed us to measure line-intensity ratios from species other than C III and provided us with consistency checks for the temperature determination. In addition, since this was the same mixture as that used in the investigations of the particle velocities[15] and the plasma composition,[14] it allowed us to use those results in the present analysis (see Sec. IV). We later found that the anode-plasma electron temperature was not sensitive to the epoxy-powder composition used for the anode (see Sec. IV).

The plasma was optically thin for the lines observed in the present study. This was learned from estimates based on the measured absolute level populations[14] and observed linewidths.[15] The plasma optical thinness was also verified experimentally.[15]

III. MEASUREMENTS

In the present experiment the determination of the electron temperature from line-intensity ratios requires that the lines be from the same charge state, due to the lack of equilibration between ionization stages. The excited-level equilibration time within the same charge state and the same spin system is about 10 ns for the present plasma parameters as will be shown later. Thus, we used C III-triplet, Mg II, and Al III levels to determine the electron temperature.

In most of the experiments reported here the line emission was collected from the entire anode plasma in a single discharge (spatially resolved measurements will be discussed in Sec. IV D). To this end the entire plasma, which is less than 3 mm wide,[15] was imaged (10× demagnified) on the 360-μm-wide input spectrograph slit.

We observed the intensities of the C III 4647-Å (the upper level is $2s3p\ ^3P_2$), 4650-Å ($2s3p\ ^3P_1$), 3609-Å ($2s5d\ ^3D$), 3889-Å ($2s5f\ ^3F_4$), and 3886-Å ($2s5f\ ^3F_3$) lines; the Mg II 2796-Å ($3p$), 2803-Å ($3p$), 2798-Å ($3d$), 2937-Å ($4s$), 4481-Å ($4f$), and 3105-Å ($5f$) lines; and the Al III 3602-Å ($4p$), 5723-Å ($4p$), 4529-Å ($4d$), 3713-Å ($5s$), 4150-Å ($5f$), 4480-Å ($5g$), 4904-Å ($7f$), and 3981-Å ($8f$) lines. The intensities of a C III line (4647 Å), a Mg II line (2796 Å), and an Al III line (3602 Å) are shown as a function of time in Fig. 2. Note that the line emission

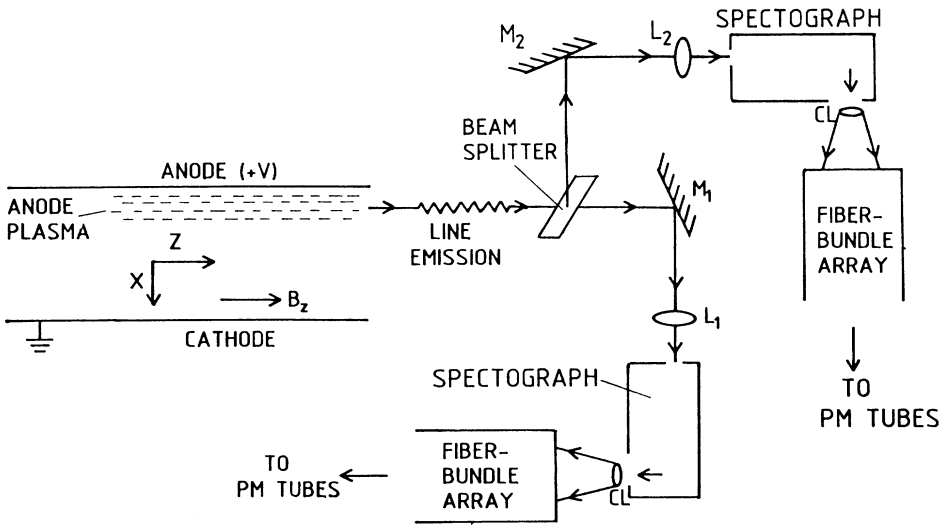

FIG. 1. Illustration of the optical arrangement. The beam splitter splits the light into two portions, each directed by a mirror and a lens (M_1 and L_1, respectively, for one portion and M_2 and L_2 for the other) to a spectroscopic system. The distance from the anode of the observed region is varied for each system by moving the corresponding mirror.

starts rising at $t_0 \approx 20$ ns after the start of the diode voltage pulse. At $t \simeq 50$ ns the plasma was found to occupy a region about 1.5 mm wide near the anode surface (see Ref. 15). Obviously, all the measurements to be presented here refer to the period $t > t_0$. The line intensities rise to a plateau that prevails between about 65 and 100 ns. The line intensities were usually reproducible to within 30%.

The population n_u (divided by the degeneracy) of the upper level feeding a transition from the level u to the level l is proportional to $I/[A_{ul} g_u R(\lambda)]$, where I is the measured line intensity expressed by the total current of the photomultiplier tubes, A_{ul} is the Einstein coefficient, g_u is the degeneracy of the upper level ($g_u = 2J+1$), and $R(\lambda)$ is the system sensitivity for the wavelength λ given by amperes per number of photons emitted from the plasma per unit time. The ratio between the populations of two levels, u_1 and u_2, observed in a single discharge using the spectrographs 1 and 2, respectively, is obtained by

$$\frac{n_{u_1}}{n_{u_2}} = \frac{I_1/[A_{ul_1} g_{u_1} R_1(\lambda_1)]}{I_2/[A_{ul_2} g_{u_2} R_2(\lambda_2)]} .$$

Note that throughout the entire paper we refer to level populations divided by the degeneracy.

Measured level-population ratios for C III, Mg II, and Al III are shown in Fig. 3. The error in the line-intensity ratio, ±30%, results from the uncertainty in the photomultiplier-tube response and the uncertainty in the response of the spectroscopic systems relative to each other. The line-intensity ratios are measured with this accuracy only for $t \gtrsim 40$ ns. For earlier times the error was about ±50% due to the rise in the line intensities. The temporal changes in the ratios are small for $t \gtrsim 50$ ns. Also, they reproduced to within 20%.

We verified the absence of impurity-line effects by several methods. (1) For multiplet lines we observed two lines of the multiplet whenever they were spectrally resolvable. The scaling of the intensity with $g_u A_{ul}$ provides a confirmation of the absence of impurity effects. (2) C III and Al III line ratios were also measured for a pure epoxy anode. The similarity of the results for both anodes precluded interference by lines of the admixed elements (Mg,Ca,Si,Na). (3) The effect of adsorbate lines was also examined by observing a few line intensities of H, O II, O III, N I, N II, and N III. This allowed us to locate strong lines of these species and to avoid measurements of nearby lines. Similar precautions have been taken with respect to lines of the admixed elements. (4) An impurity line 0.1 Å away from an observed line could be separated by our fiber-channel array.

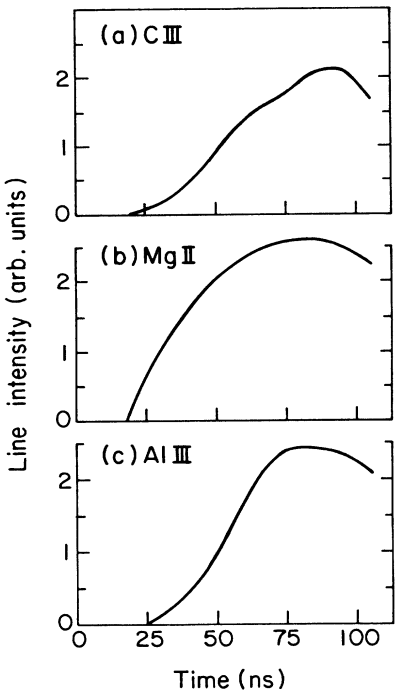

FIG. 2. Measured intensities of C III (4647-Å), Mg II (2796-Å), and Al III (3602-Å) lines as a function of time given in (a), (b), and (c), respectively. The diode voltage pulse starts at $t = 0$. Light is collected from the entire plasma.

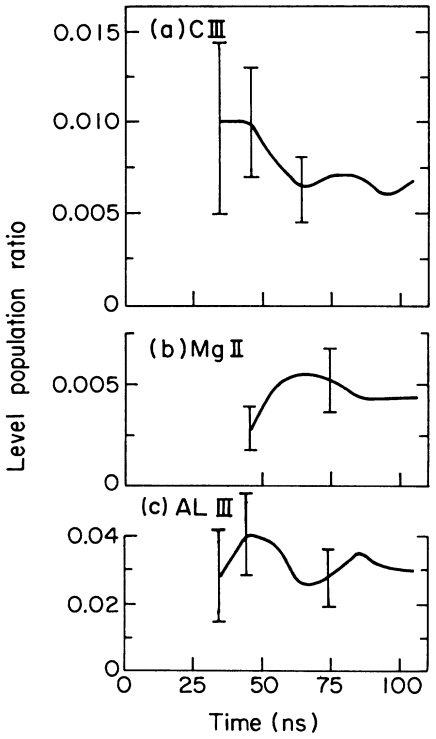

FIG. 3. Level-population ratios, each measured in a single discharge, as a function of time. All populations are divided by the degeneracy as throughout the entire paper. The uncertainty in the ratio for $t \gtrsim 40$ ns is ±30% as indicated. (a) C III—the $2s5f\,^3F_4$ population (obtained from the 3889-Å line) to the $2s3p\,^3P_2$ population (4647 Å); (b) Mg II—the $5f\,^2F$ population (3105 Å) to the $3p\,^2P_{3/2}$ population (2796 Å); (c) Al III—the $7f\,^2F$ population (4904 Å) to the $4p\,^2P_{3/2}$ population (3602 Å).

IV. DATA ANALYSIS

A. Time-dependent collisional-radiative code

The measured line intensities were analyzed with the aid of a collisional-radiative code that determines the level populations as a function of time by solving rate equations of various atomic processes for given initial particle densities. A full description of the code and its use in the analysis of fast changes in the plasma will be given in a separate publication. Here, we will only give a general discussion and specify for each species the rates used for the various atomic processes.

The code uses time-dependent electron density $n_e(t)$ and temperature $T_e(t)$ that are treated as input parameters for these calculations. The electron velocity distribution is assumed to be Maxwellian for these calculations. This is based on the electron self-collision time of about 0.1 ns for our anode-plasma parameters, which is much shorter than the time scale on which the plasma parameters are believed to change and the time scale on which free electrons are produced by ionization. In the code, each two adjacent atomic or ionic species are coupled through ionization and radiative or three-body recombinations. Atomic levels within each species are coupled through electron collisional excitation and deexcitation, and through spontaneous radiative decay. In the calculation for carbon, dielectronic recombination into $2pnl$ excited states of C III has also been included.[18,19] Recombination is, however, insignificant for the present plasma parameters and time scale.

Our Mg II model includes 42 levels of $n=3$ through $n=11$ for Mg II and one level (the ground state) for Mg III. For levels of $n=6$ to 11 the $l \geq 6$ levels were accounted for by increasing the statistical weight of the $l=5$ (g) level to include the degeneracy of these levels. The Al III model consists of 47 levels for Al III, $n=3$ through $n=12$ levels, and the Al IV ground state. We verified that the calculated level populations were insensitive to further increase in the number of levels used by adding the $n=13$ to $n=15$ levels as hydrogenic levels. The change in the level populations due to the inclusion of more levels was a few percent. The oscillator strengths for Mg II and Al III were taken from the calculations of Lindgard and Neilsen,[20] which agree with the values tabulated in Ref. 21. Ionization and excitation rates are taken from Post and Jensen.[22]

The C III code contains 42 levels for C III, $n=2$ through $n=5$ levels, and five levels for C IV. Ionization rates for C III are obtained using semiempirical fits to recent cross-section data, as is described in Ref. 23. Excitation rates for both spin-allowed and spin-forbidden transitions among the 14 lowest levels are given in Ref. 24. Transition rates among higher levels are calculated from the expressions given in Ref. 22, using oscillator strengths given in Refs. 21 and 25. The transition rates of Refs. 22 and 24 for the 14 lowest levels agree to within a few tens of percent.

In the case of C III high-n levels were accounted for by increasing the degeneracy of the $n=6$ level to include the sum of hydrogenic degeneracies ($2n^2$) up to the reduced continuum limit.[9] This prescription for treating the high-n levels was checked by replacing a group of hydrogenic levels of $n=6$ to $n=10$ with a single level with the appropriate degeneracy. Populations below $n=6$ were found to be unaffected while the population of the single level was $\simeq 20\%$ less than the previous total of the levels $n=6$ through $n=10$.

The effects of optical thickness on level populations were also examined in our calculations. The densities of the various species were determined[14] from the absolute line intensity measurements. For this determination the plasma was first assumed to be optically thin for all transitions. The calculated populations were then used to examine the self-absorption of the various lines. For this examination we used the observed[15] spectral profiles of lines of negligible self-absorption (the absence of self-absorption for these lines was verified experimentally[15]). The profiles were found to be close to Gaussian, dominated by Doppler broadening. The measured ratios $\lambda/\Delta\lambda$ (about 10^4) between the line wavelength and the line full width at half maximum (FWHM) for the various species were used to calculate the self-absorption for all lines treated in the code. It was found that the plasma was mildly thick for the first resonances of C II ($2s2p^2\,{}^2P - 2s^2 2p\,{}^2P$) and C III ($2s2p\,{}^1P - 2s^2\,{}^1S$). The radiation escape factors and the resulting effective change in the Einstein coefficients for the self-absorbed lines were calculated using the treatment described by McWhirter.[29] The calculation was then iterated until the level populations converged. This procedure increased the population of the C III first-excited level by only 10% (relative to the case of optical thinness) and modified the line ratios relevant for the electron-temperature determination by less than 2%. Therefore, optical thickness effects are determined to have a negligible effect on the calculated line-intensity ratios.

B. Determination of the electron temperature

We now use our code to calculate the level populations as a function of time. We assume a single (average) value for the electron temperature T_e. The electron density required for the calculations is taken from our measurements based on the observation of the Stark and Doppler broadening of the H_α and H_β lines.[15] Our observed electron-density axial distributions are shown in Fig. 4(a) for five different times. For the calculations we use the spatially averaged time-dependent electron density $\bar{n}_e(t)$ [shown in Fig. 4(b)] obtained from the electron-density distributions. We will later discuss the low sensitivity of the calculations to this simplifying assumption.

In this report we address the time history of the line intensities and the line-intensity ratio only up to $t \approx 95$ ns. The line-intensity ratios at later times (after the pulse) are influenced by changes in the electron density and are discussed separately.[14]

In order to examine the time scale of the excitation processes for our parameters the level populations and level-population ratios were calculated as a function of

time for C III, Mg II, and Al III. In these calculations $T_e = 7$ eV and $n_e = 2.3 \times 10^{15}$ cm^{-3} were used, and the initial conditions for each species were an instantaneous puff of ions released in their ground state at $t = 0$. It is found that the C III triplet level populations rise in about 40 ns due to the relatively slow rate of the triplet-level equilibration with the C III singlet ground state. The ratio between the triplet-level populations reaches nearly a constant value at $t \simeq 40$ ns. The Mg II and Al III excited levels, since they are of the same spin system, equilibrate faster with their ground states. The excited-level populations reach a maximum and the level-population ratios reach relatively constant values in a few nanoseconds after the initial particle supply (note that these ratios are significantly different from their steady-state values, as will be shown below).

The assumption that the plasma inventory stems from an instantaneous release of material early in the pulse results in strong disagreement with line-intensity measurements (more specifically with the rise and the plateau of the line intensities as shown in Fig. 2) for various neutrals and ions no matter what electron temperature was assumed. This is discussed in detail in Ref. 14. The rise and the plateau of the line intensities, as those shown in Fig. 2, were much more satisfactorily explained for all observed lines of neutral particles, singly charged ions, and doubly charged ions by assuming that the plasma is being continuously enriched during the diode voltage pulse by material flowing into it, evidently from the anode surface. This assumption was also consistent with the temporal rise of the areal density of the plasma electrons obtained from the Stark-broadening measurements. A simple form, parabolic in time, of the material continuous-source term was fitted to the observed line intensities with the amplitude determined quantitatively for each species using the absolute values of the line intensities. We will, therefore, determine the electron temperature by comparing the observed line-intensity ratios to ratios calculated using a continuous material source. The material flow into the plasma is expected to continuously alter the level-population ratios, as analyzed below.

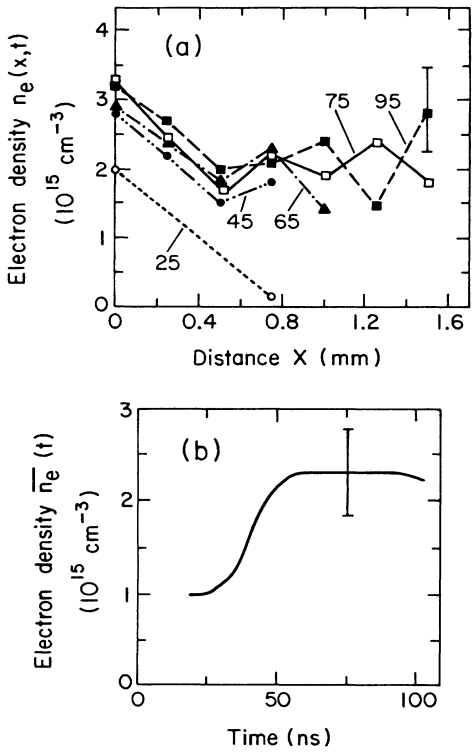

FIG. 4. (a) Measured electron density as a function of distance x from the anode surface for five times, given in nanoseconds. The spatial resolution is 0.3 mm. The data points are connected by straight lines. (b) Position average electron density $\bar{n}_e(t)$ as a function of time. The errors in (a) and (b) are $\pm 20\%$ as indicated.

The source terms obtained in Ref. 14 were

$$S(i) = A(i)\{(t - t_0)/19 - [(t - t_0)/38]^2\} \ \frac{\text{particles}}{\text{cm}^2\,\text{ns}} , \quad (1)$$

where $A(i)$ is the amplitude for species i and t is given in ns. This parabolic function has its zeros at $t = t_0 = 20$ ns (the time at which the plasma is first observed, see Sec. III) and at $t = t_0 + 76 = 96$ ns (which is near the end of the diode voltage pulse).

The level populations and the level-population ratios addressed in Figs. 2 and 3 are calculated using the parabolic source terms [Eq. (1)] and shown in Fig. 5 for $T_e = 7$ eV. Due to the continuous ion supply the excited-level populations and the level-population ratios increase in time and reach nearly constant values later than in the case of instantaneously ion supply that is discussed above. The level-population ratios for Mg II and Al III become nearly constant about 30 ns after t_0, i.e., at $t \simeq 50$ ns. The C III triplet-level population ratio rises for longer times. However, during the last 35 ns of the pulse (i.e., $t \simeq 60$–95 ns) the ratio changes by only 20%. Therefore, we shall use these line-intensity ratios to determine the electron temperature only for $t \simeq 60$ to 95 ns. The observed line-intensity ratios are approximately constant in this period of time (see Fig. 3), consistent with these calculations and with the assumption of a constant electron temperature.

For the determination of the electron temperature it is important that the line-intensity ratios are insensitive to the exact form of the source terms. To demonstrate this we give in Fig. 6 the level populations and the level-population ratios calculated for C III, Mg II, and Al III for two other source terms: a constant source and a source that varies as t^2. While the temporal variation of the level populations for C III, Mg II, and Al III differ significantly for the different sources, the excited-level population ratios, due to the relatively fast excited-level equilibration, are less sensitive to the source form. At late times ($t \simeq 50$ ns) the ratios for the two sources are close to within 20% for C III and 10% for Mg II and Al III. However, as shown in Ref. 14, a source that varies as t^2 is very unlikely. The actual material source forms are close to the parabolic form given in Eq. (1), which gives ratios closer to those of the constant source than to those of the t^2 source. Thus, we estimate that even for

C III the uncertainty in the exact form of the source term produces a small effect on the determined level-population ratio. The small sensitivity of the level-population ratios to the ionic source form and the slow temporal variation in the population ratios for $t \gtrsim 60$ ns shown in Fig. 6 occur over the entire temperature range presently considered, $4 < T_e < 10$ eV.

We now determine the electron temperature for the time period $60 < t < 95$ ns. The electron temperature was determined from the populations of the C III $2s5d\ ^3D$ and the $2s5f\ ^3F$ levels relative to that of the $2s3p\ ^3P$ level, observed at this period of time, as shown in Fig. 7. The population of the ^3D level (lies at 42.8 eV) was obtained from the 3609-Å line intensity (see the level scheme given in Fig. 7) and the population of the ^3F level (43.0 eV) from the intensities of two lines in the multiplet: the 3889- and 3886-Å lines. The population of the ^3P level (32.2 eV) was obtained from the intensities of the two multiplet lines: the 4647- and 4650-Å lines. In each discharge the ^3P population was measured simultaneously with the ^3D or the ^3F populations. The observed intensity of the 3609-Å line was corrected by 10% for the contribution of a nearby N II line. An estimate of the intensity of the latter was obtained from measurements of the intensities of the 4631-, 3594, and 3616-Å N II lines. Also shown in Fig. 7 are the calculated population ratios for $T_e = 4$, 5, 8, and 10 eV. In these calculations we use the observed spatially averaged time-dependent electron density given in Fig. 4(b), which has a value near to 2.3×10^{15} cm^{-3} during the period 60–95 ns. From these measurements we determine that T_e is between 5 and 8 eV.

Observed and calculated level populations for Mg II normalized to the $3p$ population are shown in Fig. 8 together with the level scheme. The $3p$-level population was obtained from the doublet 2796- and 2803-Å lines. The observed level-population ratios, compared to the calculations, are consistent with the electron temperature of 5–8 eV determined from the C III lines.

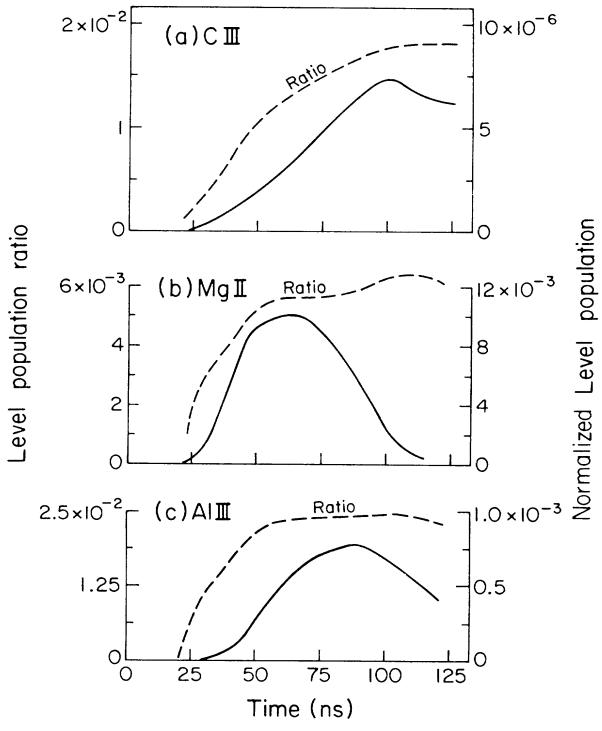

FIG. 5. Calculated level populations and level-population ratios for the parabolic supply of particles at the ground state [Eq. (1)]. The populations are normalized to the total supply of particles (up to $t = t_0 + 76$ ns $= 96$ ns). Here, $T_e = 7$ eV and the electron density is the observed time-dependent $\bar{n}_e(t)$ given in Fig. 4(b). (a) The C III $2s3p\ ^3P_2$ population and the ratio of the $2s5f\ ^3F_4$ population to the $2s3p\ ^3P_2$ population. (b) The Mg II $3p\ ^2P_{3/2}$ population and the ratio of the $5f\ ^2F$ population to the $3p\ ^2P_{3/2}$ population. (c) The Al III $4p\ ^2P_{3/2}$ population and the ratio of the $7f\ ^2F$ population to the $4p\ ^2P_{3/2}$ population.

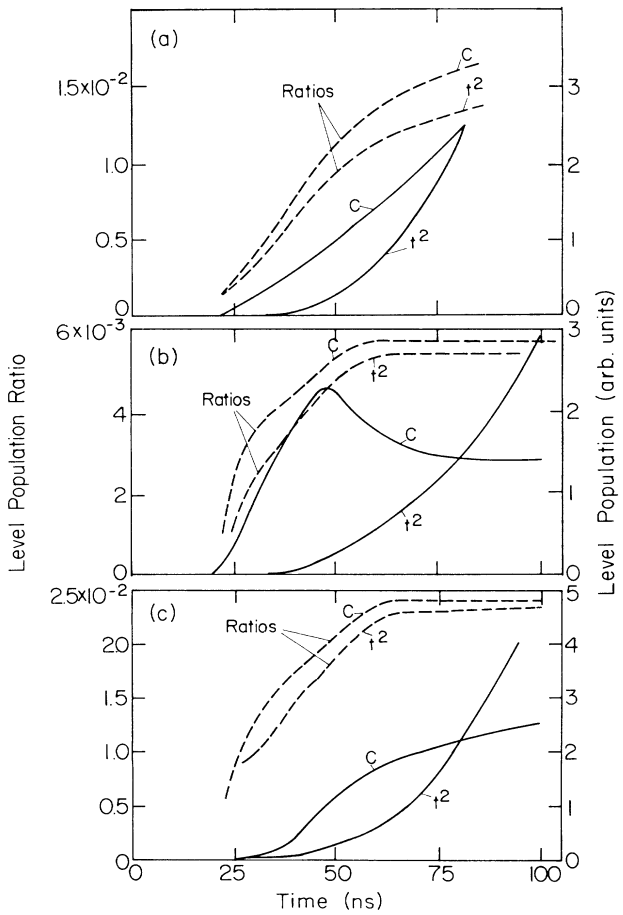

FIG. 6. Calculated populations and level-population ratios for two-particle source terms: a source constant in time (marked by C) and a source that varies as t^2. The populations for the two sources are normalized to each other at $t = 80$ ns. Here, $T_e = 7$ eV, and $\bar{n}_e(t)$ is as in Fig. 4(b). (a) The C III $2s3p\ ^3P_2$ population and the ratio of the $2s5f\ ^3F_4$ population to the $2s3p\ ^3P_2$ population. (b) The Mg II $3p\ ^2P_{3/2}$ population and the ratio of the $5f\ ^2F$ population to the $3p\ ^2P_{3/2}$ population. (c) The Al III $4p\ ^2P_{3/2}$ population and the ratio of the $7f\ ^2F$ population to the $4p\ ^2P_{3/2}$ population.

Measurements of Al III line-intensity ratios were found to be inconsistent with the calculations. We conjectured that an aluminum plasma formed near the aluminum ribs of the anode may be different from the entire anode plasma, thus affecting the spatially averaged level-population ratios observed in Al III. Therefore, for determining the electron temperature from Al III lines we used an anode made of brass (rather than aluminum) with aluminum present in the epoxy in the form of $AlNaSiO_3$ (see Sec. II). The observed Al III level populations normalized to the $4p$ population are shown in Fig. 9. The population of the $4p$ level (17.8 eV) was obtained from the 3602-Å line ($4p \rightarrow 3d$) and the 5723-Å line ($4p \rightarrow 4s$). The populations of the $5f$ and $5g$ levels (both $\simeq 23.5$ eV) were obtained from the 4150- and 4480-Å lines, respectively. The observed $5g$ population seems to be too low, as shown in Fig. 9. However, all other level populations ratios are consistent with T_e between 5 and 8 eV. We also verified that for the brass anode C III and Mg II had the same line-intensity ratios as for the aluminum anode. This was done by observing the ratio of the 3889- to the 4647-Å line intensities for C III, and the ratio of the 3105- to the 2796-Å line intensities for Mg II.

From the results for C III, Mg II, and Al III we conclude that the average T_e in the plasma at $T \approx 60$ to 95 ns is between 5 and 8 eV.

Note the large difference between the presently calculated level-population ratios and those given by steady-state calculations. For example, for $T_e = 7$ eV, our calculated steady-state populations of the C III $2s5f\ ^3F$ level ($\simeq 43$ eV), the Mg II $5f$ level ($\simeq 13$ eV), and the Al III $7f$ level (25.9 eV), normalized as in Figs. 7, 8, and 9, respectively, are larger by factors of 2, 11, and 4, respectively, than the corresponding populations given in Figs. 7–9. This emphasizes the need for time-dependent calculations and measurements for the determination of the electron temperature in such pulsed plasmas.

The uncertainty in the time history of the electron temperature in the initial stage of the pulse has little or no effect on our determination of the electron temperature due to the short excited-level equilibration time (it is the ionization relaxation that is mainly responsible for the difference of the excited-level populations from the steady-state values[9]). Using our time-dependent code we verified that the excited-level populations respond to step changes in T_e in a few nanoseconds. The sensitivity of the calculated population ratios to the uncertainty of

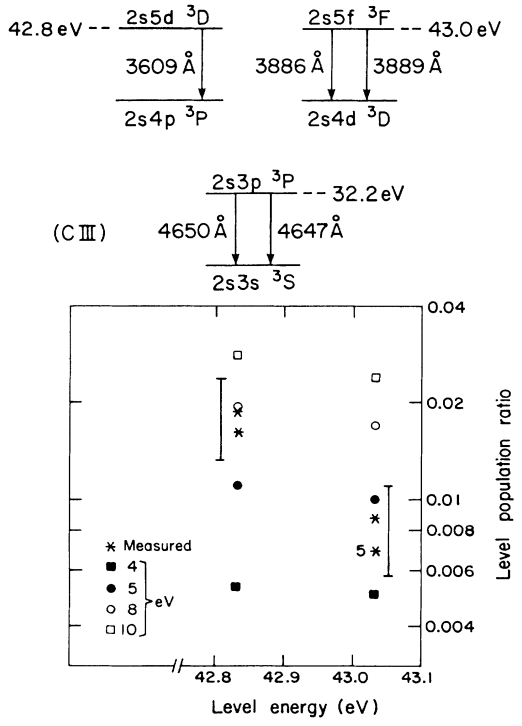

FIG. 7. Measured populations of the C III triplet levels (see the level scheme) $2s5d\ ^3D$ (lies at 42.8 eV) and $2s5f\ ^3F$ (43.0 eV), averaged between $t = 60$ and 95 ns, normalized to the population of the $2s3p\ ^3P$ level (32.2 eV). All level populations are divided by the degeneracies. Different data points shown were obtained from repeated discharges. The data point marked 5 for the ^3F level represents five measurements that were close to within 10% to each other. The uncertainty in the ratios is ±30% as indicated by the error bars near the data points. Also shown are calculated normalized level populations for four electron temperatures $T_e = 4$, 5, 8, and 10 eV at $t \simeq 80$ ns. For the calculations, the parabolic ion source [Eq. (1)] is used together with the observed time-dependent position-averaged electron density $\bar{n}_e(t)$ [see Fig. 4(b)].

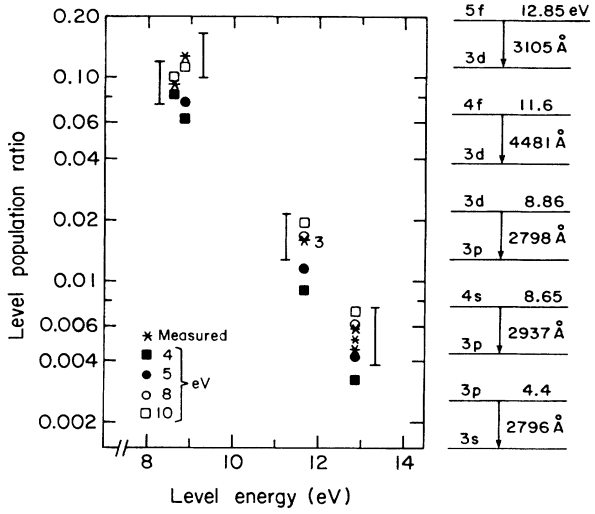

FIG. 8. Measured Mg II level populations normalized to the population of the $3p$ level (that lies at 4.4 eV), averaged between $t = 60$ and 95 ns. The observed lines and the level energies in electron volts are given in the level scheme. The different data points for the $5f$ level are from repeated measurements. The data point marked 3 for the $4f$ level represents three measurements that agreed to within 10%. The uncertainty is ±30% as indicated by the error bars near the data points. Also shown are the calculated normalized populations for $T_e = 4$, 5, 8, and 10 eV at $t \simeq 80$ ns, using the parabolic source [Eq. (1)] and the electron density $\bar{n}_e(t)$ given in Fig. 4(b).

±20% in the average electron density $\overline{n_e}(t)$ was also examined. This gave an uncertainty of ±10% in the level-population ratios, which corresponds to an uncertainty of ±0.5 eV in T_e.

In order to estimate the sensitivity of our temperature determination to uncertainties in the process rates used in the code, we recalculate the level populations of C III using different decay rates and excitation rates. Decreasing all decay rates A_{ik} by 30% (and not changing the excitation and deexcitation rates), which is a reasonable estimate for their average uncertainty, results in a 10% increase in the triplet ratios used in determining the temperature. Decreasing all excitation rates and deexcitation rates by 30% (and not changing A_{ik}) results in ≃20% decrease in these ratios. These changes correspond to ≃1 eV uncertainty for T_e near 7 eV. We also repeated calculations for Mg II with oscillator strengths increased by 30%, thus increasing the radiative decay rates, the excitation rates, and the deexcitation rates by 30%. This resulted in a decrease of ≃0.5 eV in the determined T_e.

Measurements of spectral intensities from Be-like ions in θ pinch[27,28] and tokamak[29] experiments have suggested that a few particular excitation and decay rates between certain levels may be incorrectly calculated by as much as a factor of 2, mostly for $n=2$ to $n=3$ transitions. However, by varying each of these particular "suspect" transi-

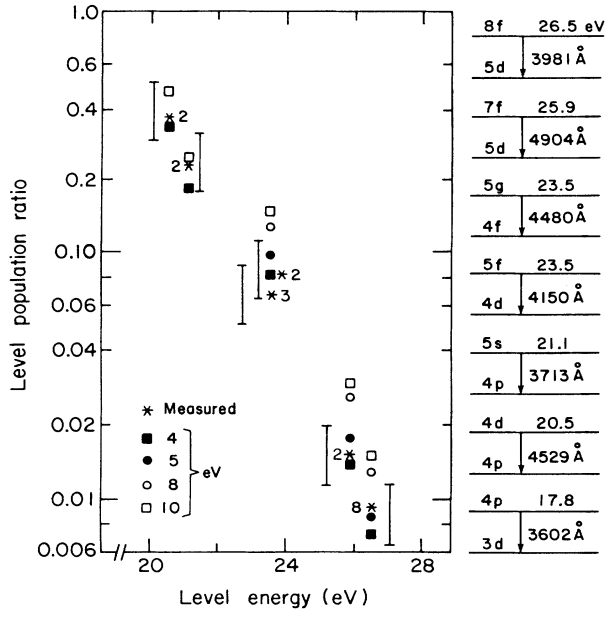

FIG. 9. Al III level populations, observed with the brass anode, normalized to the 4p level population, averaged between $t=60$ and 95 ns. The observed lines and the level energies in electron volts are given in the level scheme. The numbers near the data points are the numbers of repeated measurements that agreed to within 10%. The data points marked 2 and 3 at 23.5 eV correspond to the 5f and the 5g levels, respectively. The uncertainty is ±30% as indicated by the error bars near the data points. Also shown are calculated normalized populations for $T_e=4$, 5, 8, and 10 eV at $t\simeq 80$ ns, using the parabolic source [Eq. (1)] and the electron density $\overline{n_e}(t)$ given in Fig. 4(b).

tion rates in our C III code by a factor of 2, we found an insignificant change in the population ratios used in determining the temperature. Of course, it is possible that one or a few of the rates between higher levels, which more directly determine the population ratios used to obtain the electron temperature, are also off by a factor of 2. However, by using several line-ratio measurements we have reduced the chance of an error in the temperature determination. Also, we have obtained a similar value for T_e (5–8 eV) from C III, Mg II, and Al III line-ratio measurements.

We now discuss a discrepancy between our measurements and the code calculations. We also measured the populations of C III singlet levels $2p^2\,{}^1D$, $2p3p\,{}^1D$, $2s5d\,{}^1D$, and $2s5f\,{}^1F$ from the intensities of the 2297-, 4326-, 4122-, and 4056-Å lines, respectively. Except for the lowest $2p^2\,{}^1D$ level (that lies at ≃18 eV) the relative populations of all observed singlet and triplet levels (all these levels lie above 32 eV) agreed reasonably well with the calculations using $T_e=5$–8 eV. However, the observed ratio between the populations of each of these levels and the $2p^2\,{}^1D$ population was about 5 times larger than the calculated ratio, even for $T_e=8$ eV. This discrepancy is not clear to us as yet. We do believe, however, that it results from the fact that, given the total C III density, the code predicts too low values for the populations of the high levels (the observed levels that lie above 32 eV) rather than predicting a too high value for the $2p^2\,{}^1D$ level. This is mainly due to our greater confidence in the rates amongst the lower $n=2$ to $n=2$ transitions, a point discussed in detail in Ref. 14.

We examined whether the ratio between the high-level populations and the $2p^2\,{}^1D$ population results from recombination of C IV. For these estimates we assumed a C IV density of 2×10^{14} cm^{-3} that is consistent with the total plasma density. The recombination processes (dielectronic,[18,19] three-body, and radiative recombination) were found to increase the ratios of the high-level populations to the $2p^2\,{}^1D$ population by only 20%. Charge-exchange recombination of C IV with H has been shown[30] to have a relatively large cross section ($\simeq 2\times10^{-15}$ cm^2 at 5 eV) and could, in principle, be an important mechanism of populating the high levels assuming this C IV density. However, the C IV density is probably smaller than the value assumed above. This is partially due to the fact that very little C IV is produced at these temperatures from ionization. Also, from Table I of Ref. 14, it was found that the ejection rate of C III from the anode is smaller than that of C II. As discussed in Ref. 14, since the C III ionization rate on the anode surface is much smaller than that of C II, we might further expect a reduction in the flux of C IV ions into the plasma. Therefore, it is likely that due to low concentrations of C IV in the plasma charge-exchange recombination effects are also small. Thus, we have no satisfactory explanation for the high population densities of the C III higher levels.

C. Dependence of T_e on the anode epoxy admixture and on the magnetic field

We examined the sensitivity of the electron temperature to the presence of various compounds as additives in

the epoxy used for the dielectric anode (see Sec. II) by also determining the temperature for a pure epoxy anode. The line-intensity ratios measured for the pure epoxy anode were (1) the ratio between intensities of the three C III triplet lines, 3609-, 3889-, and 3886-Å lines, and that of the 4647-Å line, and (2) the ratios between the intensities of the two Al III lines, 4904 Å and 4150 Å, and that of the 3602-Å line. Within the experimental uncertainty the admixtures used for the anode epoxy did not affect the line-intensity ratios in C III and Al III.

The effect of the strength of the applied magnetic field B_z on the electron temperature was examined by measuring the intensity ratios of the Mg II 3105- and 2796-Å lines for B_z between 5.5 and 9.0 kG. The ratios obtained were the same within the experimental uncertainty.

D. Electron temperature as a function of distance from the anode surface

In this section we report measurements of line-intensity ratios as a function of the distance x from the anode made in order to determine the temperature gradient across the plasma. For these measurements the C III ions were most suitable since these ions propagate to the outer region of the plasma[14] due to their relatively high velocities[15] and long ionization times.

The average C III propagation velocity in the plasma is about 1 cm/μs,[15] i.e., the C III propagation distance during the level-equilibration time (a few nanoseconds) is small with respect to the plasma thickness. Thus, measurements of a line-intensity ratio as a function of the distance x from the anode surface should indicate axial variations of the electron temperature.

We, therefore, measured simultaneous intensities of C III triplet lines for various axial positions in the plasma. The spatial resolution (in the x direction) was set in these experiments to be about 0.5 mm by using 30-μm-wide input slits for the spectrographs (the demagnifications of the lenses L_1 and L_2 remained about 10). We performed two series of discharges. We measured the intensity ratio of the 3889- and 4647-Å lines in one series and the intensity ratio of the 3609- and 4647-Å lines in the other (see the scheme in Fig. 7). In these experiments we were especially interested in obtaining the temperature gradients at the end of the voltage pulse (see discussion in Sec. IV E). Thus, we present the line-intensity ratio averaged over $75 \lesssim t \lesssim 95$ ns. The observed line-intensity ratios as a function of the distance x from the anode surface for this period of time are given in Figs. 10(a) and 10(b), respectively. It is seen that the intensity ratios for both line pairs are constant to within the experimental uncertainty across the entire plasma. For $0.5 \leq x \leq 1.5$ and $75 \leq t \leq 95$ ns the measured electron density may vary within $\pm 20\%$ (which is the uncertainty in the electron-density measurements). This may affect the axial dependence of the line-intensity ratios by about $\pm 10\%$, which is within the experimental uncertainty of the line-intensity ratios. Accounting for the measurement uncertainty, this allows us to conclude that for $t = 75-95$ ns the electron-temperature variation for $x > 0.5$ mm is < 1 eV. The implication of this result will be discussed in Sec. IV E.

In order to further support this result we measured the intensity ratio of the 4326-Å (the upper level is $2p3p\ ^1D$) to the 2297-Å ($2p^2\ ^1D$) singlet lines as a function of x, see Fig. 10(c). The 4326-Å line, due to its larger intensity relative to the high triplet-level lines, allowed the measurements to be extended to $x = 1.6$ mm. The observed line-intensity axial distributions for the various ions in the plasma indicate that this distance is very probably close to the entire extent of the plasma. The intensity ratio was measured for $0.3 \lesssim x \lesssim 1.6$ mm, showing no variation over this range. A temperature change of 1 eV would have caused a change of 70% in the line-intensity ratio due to the large energy differences (23 eV) between these singlet levels. Unfortunately, it is not certain whether we can use this ratio for a quantitative determination of the electron temperature, due to the discrepancy between the calculated and the experimental ratios of the population of the $2p^2$ level (the upper level of the 2297-Å line) to all other level populations observed (see Sec. IV B). Here, we use, however, only the change in the ratio. The fact that this ratio also has little or no spatial variation further supports our conclusion, based on the triplet ratios, that for $75 < t < 95$ ns the electron temperature across the plasma is very uniform.

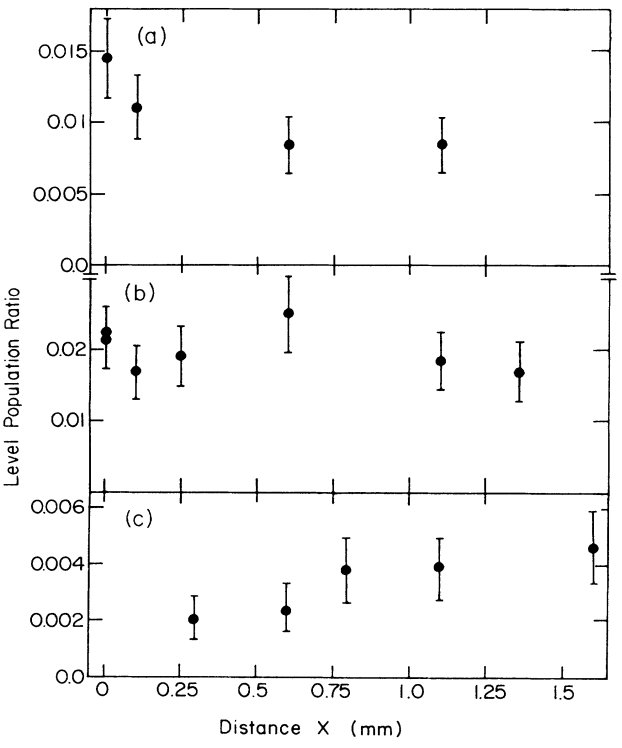

FIG. 10. Ratio of C III level populations as a function of distance x from the anode surface (the anode surface is at $x = 0$) averaged over $t = 75$ to 95 ns. For each position the ratio was measured in a single discharge. The spatial resolution was about 0.5 mm. (a) The ratio of the $2s5f\ ^3F_4$ population (3889-Å line) to the $2s3p\ ^3P_2$ population (4647 Å). (b) The ratio of the $2s5d\ ^3D$ population (3609 Å) to the $2s3p\ ^3P_2$ population (4647 Å). (c) The ratio of the $2p3p\ ^1D$ population (4326 Å) to the $2p^2\ ^1D$ population (2297 Å).

E. Discussion of the electron heating

We shall now analyze the electron-heating and -cooling processes in the plasma based on the presently determined electron temperature, plasma density,[15] and ion temperature.[15] For simplicity we assume a proton-electron plasma and we use a one-dimensional fluid treatment. The use of a fluid treatment is reasonably justified since the proton Larmor radius is about $\frac{1}{3}$ of the plasma thickness and the inverse proton cyclotron frequency (14 ns) is shorter than the pulse length.[15]

A source for the electron Ohmic heating in the plasma is the current j_{yd} induced in the $-y$ direction by time-dependent $E_x B_z$ electron flow in the diode acceleration gap. In order to estimate these induced currents the temporal variation of the magnetic-field $B_a(t)$ on the anode side must be known.

The magnetic field $B_a(t)$ during the pulse was obtained by the observation of Zeeman splitting in the anode plasma. It was then found[17] to agree with an estimate based on the observed time-dependent ion-current density $J_i(t)$ and a relation between $B_a(t)$ and the magnetic field $B_c(t)$ on the cathode side that was inferred using measured electric field distribution in the diode acceleration gap[31] and the formula given by Mendel and Quintenz.[32] In these experiments, $J_i(t)$, observed using charge collectors outside the diodes in various locations in the ion beam, was found to be well approximated by $J_i(t)=100\{(t-t_0)/35-[(t-t_0)/70]^2\}$, where $J_i(t)$ is in amperes per square centimeter, t is given in nanoseconds, and $t_0=20$ ns. We thus obtain the functional form for $B_a(t)$ as described in Ref. 17 to obtain the rise $[B_a(t)-B_{\rm app}]$ of the magnetic field on the anode side.

To obtain the magnetic field profile in the plasma we assume a uniform semi-infinite plasma at $\xi \le 0$ mm, where ξ is a coordinate along the x direction and $\xi > 0$ is the diode gap. The magnetic field $B_a(t)$ is imposed at $\xi=0$. For the solution of the magnetic field profile in the plasma the assumption that the plasma is semi-infinite is justified since there is a conductor (aluminum plate) behind the anode-dielectric sheet. Neglecting the displacement current in Ampere's law and assuming a constant plasma conductivity the equation for the magnetic field $B_z(\xi,t)$ for a one-dimensional plasma bounded in the ξ direction is

$$\frac{\partial B_z}{\partial t}=D\frac{\partial^2 B_z}{\partial \xi^2}\ , \tag{2}$$

where $D=c^2/4\pi\sigma$ is the magnetic diffusion coefficient, c is the speed of light, and σ is the plasma conductivity. We solve this equation with the initial and boundary conditions $B_z(\xi, t=t_0)=B_{\rm app}$ and $B_z(\xi=0, t)=B_a(t)$, respectively. The neglect of the convective term in Eq. (2) will be discussed below.

We first estimate the induced current and the Ohmic heating assuming a classical plasma conductivity σ.[16] We use a constant electron temperature $T_e=7$ eV. The magnetic field from Eq. (2) is then used to give the current density by

$$\frac{4\pi}{c}j_{yd}=-\partial_\xi B_z\ . \tag{3}$$

The calculated distribution of the current density (for a classical conductivity) is shown in Fig. 11(a) for $t=95$ ns. Note that the induced current density decays by a factor of about 2, 2 mm into the plasma ($\xi=-2.0$ mm).

The Ohmic heating rate $H(\xi,t)=j_{yd}^2/\sigma n_e$ per electron in the plasma, is now calculated using $n_e=2.2\times10^{15}$ cm^{-3}, which is the average electron density in the plasma (see Sec. IV). In Fig. 11(b) we plot the calculated total electron heating $P(\xi,t)=\frac{2}{3}\int_0^t H(\xi,t')dt'$ up to time t for two positions: $\xi=0$ and $\xi=-1$ mm. It is seen that at $t=95$ ns the current induced by the electron flow in the diode gap would increase the electron temperature by about 7 eV in the outer plasma region ($\xi=0$), resulting in a temperature gradient of about 5 eV in the outer 1-mm-wide region of the plasma. This would occur if the effects which tend to reduce the temperature gradient are small as discussed below.

Measurements of the time-dependent component of the magnetic field in the plasma by the observation of Zeeman splitting of emission lines[17] agreed with the value of $B_a(t)$ estimated here. We estimate the error in $B_a(t)$ due to the uncertainty in J_i and the average ion mass and charge in the beam to be $\pm25\%$. The uncertainty in $B_a(t)$ results in an uncertainty of $\pm50\%$ in the temperature gradient calculated in Fig. 11(b). Note that in Eq. (2)

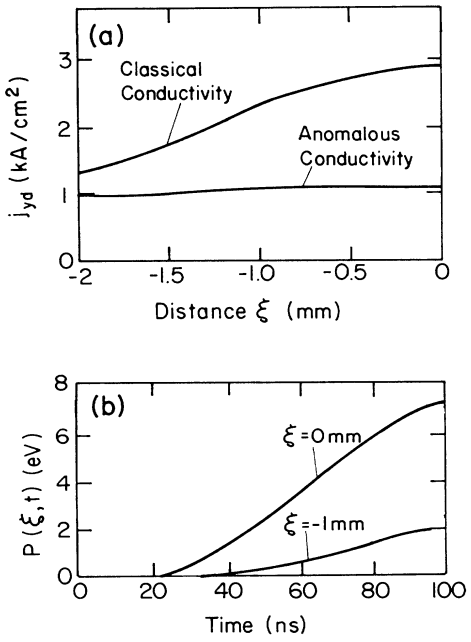

FIG. 11. (a) Calculated induced current distribution as a function of distance into the plasma for $t=95$ ns assuming a classical plasma conductivity with $T_e=7$ eV. Also shown is the current distribution for an anomalous electron conductivity for the same time. The plasma occupies the $\xi \le 0$ space. (b) The total electron heating $P(\xi,t)$ due to the induced currents up to a time t as a function of t for $\xi=0$ and -1 mm into the plasma, assuming a classical conductivity.

we neglected the convective term. Including the convective term and using the observed plasma expansion velocity V_x of about 1 cm/μs (Ref. 15) gives a temperature gradient in the plasma larger by 30% than for the case of $V_x=0$. We also note that in the calculation of the electron heating we neglected the contribution of the ion current drawn from the plasma since it is much smaller than j_{yd}.

The electron heating may be balanced by electron-energy losses due to inelastic collisions. These collisions include ionizations and excitations (free-free transitions are negligible for the present parameters[9]). The calculation of the electron cooling is given in Ref. 14. The major electron-energy losses were found to be due to hydrogen ionization and due to impact excitations of C II and C III. The ionization and the excitation processes cause spatially averaged electron cooling of $\simeq 4$ and $\simeq 3$ eV during the pulse. The electron-energy losses due to ionization decrease with the distance x from the anode due to the decrease in the hydrogen density with the distance.[14] The energy losses due to impact excitations depend weakly on the electron temperature for the temperature range considered. Hence, these processes of electron cooling are not expected to reduce the temperature gradient caused by the heating due to the induced currents.

The temperature gradient in the plasma can, in principle, be reduced by electron thermal convection and conduction. Due to the relatively large currents in the plasma in the y direction the electron heat convection is much faster than the heat conduction. The characteristic electron classical heat convection time is $t_c = L_T(\omega_{ce}/\nu_{ei})/(j_{yd}/en)$,[16] where L_T is the scale length of the temperature gradient. This gives about 700 ns for the present parameters and $L_T=1$ mm. The uncertainty in t_c due to the uncertainty in j_{yd}, in the observed n_e, and in T_e is less than a factor of 2. This long thermal convection time, resulting from the electron magnetization ($\omega_{ce}/\nu_{ei}\simeq 40$) in the magnetic-field-penetrated plasma,[17] implies that assuming a classical conductivity a temperature difference of about 5 eV would develop at the end of the pulse over the 1-mm-wide outer region of the plasma as discussed above.

However, the measurements of the line-intensity ratios as a function of x (see Sec. IV D) showed no increase in the electron temperature in the outer region of the plasma, with the temperature spatial variation over the plasma of <1 eV, in clear disagreement with the large temperature gradient predicted here.

In order to explain this, we use our suggestion discussed in Refs. 15 and 17 that the plasma conductivity is $\simeq 10\times$ lower than the classical conductivity, i.e., it is $\sigma_a \simeq 2\times 10^{13}\ \mathrm{s}^{-1}$. The distribution of the current induced in the plasma for this anomalous plasma conductivity is shown in Fig. 11(a) for $t=95$ ns. The current is rather uniform and much smaller than in the case of a classical conductivity. This would cause a uniform electron heating in the plasma. However, in the case of an anomalous plasma conductivity, the induced currents j_{yd} are smaller than the total current in the plasma that results from the plasma pressure gradient in the magnetic field. The total current in the plasma is estimated[15] from the observed electron temperature, ion temperature, and plasma density to be $j_y \simeq -1600\ \mathrm{A/cm^2}$, i.e., about twice the current j_{yd}. Therefore, the electron heating is mainly affected by the pressure-driven current. The axial (normal to the anode surface) dependence of the electron heating cannot be calculated in detail since the axial dependence of the plasma pressure gradient is not accurately known. However, in the presence of this anomalous plasma conductivity, it is likely that the temperature gradient in the plasma would be small, since using the total plasma current j_y estimated above, and the value of σ_a used here, the electron thermal convection time t_c is $\simeq 100$ ns, short enough to further reduce the temperature gradient. It is estimated that with such a thermal convection rate the temperature gradient would be reduced by 30%. Therefore, the assumption of an anomalous plasma conductivity appears to be consistent with the observed absence of a temperature gradient in the plasma.

We now estimate the total electron heating in the plasma. If the total Ohmic heating due to the total current j_y in the plasma and the anomalous plasma conductivity σ_a is spent on the electrons, then the electrons would heat by $\simeq 10$ eV during the 70-ns-long pulse, averaged over the entire plasma. A smaller source of electron heating is the electron-ion elastic collisions resulting from the ions being hotter [with a temperature about 25 eV (Ref. 15)] than the electrons. This source of electron heating would increase the total electron heating to about 14 eV over the pulse. The spatially averaged electron cooling due to inelastic collisions was shown in Ref. 14 to amount to $\simeq 7$ eV over the pulse. Also, with the anomalous conductivity, the thermal convection to the anode surface is estimated to reduce the net electron heating over the pulse by about 30%. Thus, to within the uncertainties, the electron heating and cooling rates can be approximately balanced, which is consistent with the near constancy observed for the electron temperature over the second half of the pulse (see Sec. IV B).

V. SUMMARY

We have determined the electron temperature in the anode plasma of a magnetically insulated ion diode to be between 5 and 8 eV by observing line-intensity ratios of three species: C III, Mg II, and Al III ions. For this determination, the time-dependent line-intensity ratios were measured in single discharges and time-dependent calculations of the ionic level populations were shown to be essential. The calculations used the measured time-dependent electron density[15] and accounted for the continuous material flow from the anode surface into the plasma.[14]

The observed electron temperature and density were used to calculate the electron Ohmic heating that results from both the plasma current due to the plasma pressure gradient in the magnetic field and the current induced in the plasma by the electron flow in the diode acceleration gap. Calculations assuming classical electron conductivity predicted electron heating dominated by the nonuniform induced currents which would result in a large temperature gradient in the plasma. This is in clear disagree-

ment with the measured spatial dependence of line-intensity ratios in the plasma which indicated a rather uniform electron temperature. However, using an anomalous plasma conductivity $\simeq 10\times$ lower than the classical conductivity gives lower and more uniform induced currents in the plasma. The electron heating then mainly results from the current due to the plasma pressure gradient in the magnetic field. This anomalous conductivity also results in a faster electron thermal convection in the magnetized[17] plasma. Thus, heating due to the pressure-gradient current and the moderately fast thermal convection are likely to lead to a uniform electron temperature in the plasma, consistent with the observations. Furthermore, it is shown that the temporally and spatially averaged electron heating calculated with the total pressure-driven current and the anomalous conductivity, together with the heating due to elastic collisions with the hotter ions,[15] is approximately balanced by the average electron-energy losses. The latter are mainly due to inelastic collisions with the plasma particles[14] and thermal convection to the anode surface. This balance between the average electron heating and cooling rates is consistent with the approximate constancy of the electron temperature observed. The anomalous plasma conductivity used here also serves to explain the fast penetration into the plasma of the time-dependent component of the magnetic field in the diode.[17] It is also a plausible explanation for the relatively fast plasma expansion rate observed, as shown in Ref. 15. A mechanism that is possibly responsible for this anomalous conductivity is the lower hybrid drift instability in the low-drift velocity regime, as previously discussed.[15] The electron drift that may drive the instability results from the plasma pressure gradient which is estimated from the observed ion temperature, plasma density,[15] and the presently determined electron temperature.

In this paper we do not discuss the implications of the observed electron temperature on the ion charge states in the plasma. This is discussed in detail in Ref. 14. In brief, the electron temperature and density result in fast ionization of neutral particles and singly charged ions so that mainly doubly charged ions and protons reach the outer (ion-emitting) region of the plasma. Also, a significant amount of protons are produced in the outer plasma region due to the ionization of the fast-moving hydrogen atoms that traverse the plasma. The electron temperature and density are shown to determine the spatial and the temporal variations of the density ratio between protons and the nonprotonic ions in the plasma.

The electron temperature in plasmas produced in pulsed-power devices significantly affects the plasma behavior and the device operation. We believe that investigations of the electron temperature in such short-lived plasmas may help to achieve a better control over the plasma properties in a variety of pulsed plasma sources.

ACKNOWLEDGMENTS

It is a pleasure to thank Z. Zinamon, A. E. Blaugrund, and H. R. Griem for critical comments and careful reading of the manuscript. We are grateful to M. Markovits and E. Nahshoni for their help in the experiments and to G. Hazak, C. Litwin, A. Fruchtman, and E. Nardi for valuable discussions. Thanks are due to E. Elias for help in the data analysis and to P. Meiri and Y. Danino for skilled technical assistance.

[1]P. Dreike, C. Eichenberger, S. Humphries, and R. N. Sudan, J. Appl. Phys. **47**, 85 (1976).

[2]S. Humphries, Jr., Nucl. Fusion **20**, 1549 (1980).

[3]J. P. VanDevender, Plasma Phys. Controlled Fusion **28**, 841 (1986).

[4]See, for example, R. B. Miller, *Intense Charged Particle Beams* (Plenum, New York, 1982), and references therein.

[5]See, for example, R. A. Meger *et al.*, in Proceedings of the Fifth International Conference on High-Power Particle Beams, San Francisco, CA, 1983, p. 330 (unpublished), and references therein.

[6]P. Ottinger, S. A. Goldstein, R. A. Meger, J. Appl. Phys. **56**, 774 (1984).

[7]C. W. Mendel, Jr., D. B. Seidel, and S. E. Rosental, Laser Particle Beams **1**, 311 (1983); C. W. Mendel, Jr., D. B. Seidel, and S. A. Slutz, Phys. Fluids **26**, 3628 (1983).

[8]T. J. Orzechowski and G. Bekefi, Phys. Fluids **19**, 43 (1976); **22**, 978 (1979).

[9]H. Griem, *Plasma Spectroscopy* (McGraw-Hill, New York, 1964).

[10]W. Engelhardt, Phys. Fluids **16**, 217 (1973).

[11]D. J. Johnson, A. V. Farnsworth, Jr., D. L. Fehl, R. J. Leeper, and G. W. Kuswa, J. Appl. Phys. **50**, 4524 (1979).

[12]D. J. Johnson, E. J. T. Burns, J. P. Quintenz, K. W. Bieg, A. V. Farnsworth, Jr., L. P. Mix, and M. A. Palmer, J. Appl. Phys. **52**, 168 (1981).

[13]D. Hinshelwood, Naval Research Laboratory Memorandum Report No. 5492, 1985 (unpublished).

[14]Y. Maron, L. Perelmutter, E. Sarid, M. E. Foord, and M. Sarfaty (unpublished).

[15]Y. Maron, E. Sarid, O. Zahavi, L. Perelmutter, and M. Sarfaty, Phys. Rev. A **39**, 5842 (1989).

[16]S. I. Braginskii, in *Reviews of Plasma Physics,* edited by M. A. Leontovich (Consultants Bureau, New York, 1965), Vol. 1, p. 205.

[17]Y. Maron, E. Sarid, E. Nahshoni, and O. Zahavi, Phys. Rev. A **39**, 5856 (1989).

[18]D. J. McLaughlin and Y. Hahn, Phys. Rev. A **27**, 1389 (1983).

[19]P. F. Dittner, S. Datz, P. D. Miller, C. D. Moak, P. H. Stelson, C. Bottcher, W. B. Dress, G. D. Alton, and N. Neskovic, Phys. Rev. Lett. **51**, 31 (1983).

[20]A. Lindgard and S. E. Nielsen, At. Data Nucl. Data Tables **19**, 533 (1977).

[21]W. L. Wiese, M. W. Smith, and B. M. Glennon, National Bureau of Standards Report No. NSRDS-NBS 4, 1966 (unpublished); W. L. Wiese, M. W. Smith, and B. M. Miles, National Bureau of Standards Report No. NSRDS-NBS 22, 1969 (unpublished); W. L. Wiese and G. A. Martin, National Bureau of Standards Report No. NSRDS-NBS 68, Part II, 1980 (unpublished).

[22]D. E. Post and R. V. Jensen, At. Data Nucl. Data Tables **20**, 434 (1977).

[23]R. D. Taylor and A. W. Ali, J. Quantum Spectrosc. Radiat. Transfer **36**, 373 (1986).
[24]Y. Itikawa, S. Hara, T. Kato, S. Nakazaki, M. S. Pindzola, and D. H. Crandall, At. Nucl. Data Tables **33**, 149 (1985).
[25]B. C. Fawcett. At. Data Nucl. Data Tables **30**, 423 (1984).
[26]R. W. P. McWhirter, in *Plasma Diagnostic Techniques,* edited by H. Huddleston and S. L. Leonard (Academic, New York, 1965).
[27]J. Lang, J. Phys. B **16**, 3907 (1983).
[28]J. Lang, R. A. Hardcastle, R. W. P. McWhirter, P. H. Spurret, J. Phys. B **20**, 43 (1987).
[29]L. K. Huang, S. Lippmann, B. C. Stratton, H. W. Moos, and M. Finkenthal, (unpublished).
[30]S. Bienstock, T. G. Heil, C. Bottcher, and A. Dalgarno, Phys. Rev. A **25**, 2850 (1982).
[31]Y. Maron, M. D. Coleman, D. A. Hammer, and H. S. Peng, Phys. Rev. A **36**, 2818 (1987).
[32]C. W. Mendel, Jr. and J. P. Quintenz, Comments Plasma Phys. Controlled Fusion **8**, 43 (1983).